Biometals (2012) 25:577–586
DOI 10.1007/s10534-012-9542-x

Secondary structure of antisense RNAβ, an internal transcriptional terminator of the plasmid-encoded iron transport-biosynthesis operon of *Vibrio anguillarum*

Daniel McIntosh-Tolle · Michiel Stork · Alejandro Alice · Jorge H. Crosa

Received: 6 March 2012 / Accepted: 15 March 2012 / Published online: 11 April 2012

Abstract RNAβ affects the transcription process of the iron transport-biosynthesis operon encoded in the pJM1 plasmid of *Vibrio anguillarum* at a stem-loop structure located in the intergenic region between the *fatA* and *angR* genes. The net result is a higher level of the *fatD*, *fatC*, *fatB*, and *fatA* moiety as compared with the longer transcript encoding those genes as well as the *angR* and *angT* genes. In this work we report the secondary structure of RNAβ determined by treatment with single and double strand specific ribonucleases as well as lead acetate followed by sequencing. The generated in vitro structural data indicated that three of the four previously described loops are in agreement with the original model, however, the alteration of loop IV as well as several other structural differences in the overall shape of the molecule led to the necessity of creating a new in silico model. Using the sites of mutations in the various loops we modeled the change in the RNAβ secondary structure induced by those mutations. Mutations of loops III and IV to their complementary bases alter the overall structure of the RNAβ significantly and increase its function while mutations in loops I and II have the opposite effect, the structure is unchanged but the activity of RNAβ decreases. This indicates that loops I and II are necessary for interaction with the target mRNA. It is possible that the structural rearrangement introduced by mutations in loops III and IV promote activity and binding in loops I and II through reducing steric hindrance or increased binding to the target. This result also indicates that the exact relative positions of the critical loops are unimportant for activity.

Keywords Antisense RNA · Iron transport · Plasmid · *Vibrio anguillarum*

D. McIntosh-Tolle · M. Stork · A. Alice · J. H. Crosa (✉)
Department of Molecular Microbiology and Immunology, Oregon Health and Science University, Portland, OR 97239, USA
e-mail: crosajor@ohsu.edu

Present Address:
M. Stork
National Institute for Public Health and the Environment, Bilthoven, The Netherlands

Introduction

The pJM1 plasmid-encoded iron transport-biosynthesis (ITB) operon includes the iron transport genes *fatD*, *fatC*, *fatB*, *and fatA*, as well as two of the anguibactin biosynthesis genes, *angR* and *angT*. We localized the promoter for the ITB operon upstream of the *fatD* gene (Chai et al. 1998; Chen et al. 1996). The operon genes are involved in the synthesis and transport of ferric anguibactin, an essential factor of virulence for the fish pathogen *V. anguillarum* (Actis et al. 1988). The ITB operon is regulated at the transcription initiation level by the chromosome-

encoded negative regulator Fur and positively regulated by the pJM1 plasmid-encoded *angR* and TAF (Chen and Crosa 1996; Wertheimer et al. 1999; Salinas et al. 1989; Tolmasky et al. 1994). We have identified two genes on the complementary strand of this operon, *rnaA* and *rnaB*, that encode two counter-transcripts, named antisense RNAα and RNAβ, respectively (Salinas et al. 1993). We have found that RNAβ plays a role in the regulatory network of the ITB operon dictating the relative abundance of the transcript corresponding to the full-length ITB mRNA. We showed that there is a reduction in the level of this whole ITB mRNA while a shorter mRNA encoding only *fatD*, *fatC*, *fatB*, and *fatA*, remains high (Stork et al. 2007). We demonstrated that these results were due to a transcription termination event between *fatA* and *angR*, with the major termination event occurring at stem-loop II (Stork et al. 2007). This stem-loop does not fall into any of the present classifications for transcription terminators suggesting a novel mechanism for the termination event within this operon. Because of the location of the *rnaB* gene and the complementary nature of the loops in both RNAs, we demonstrated that the 427-nucleotide long antisense RNAβ is an effector of transcription termination at the intergenic loop within this operon. Therefore, although all of the components for transport and biosynthesis are controlled by modulating the activity of a single promoter the antisense RNA-mediated transcription termination mechanism results in a fine-tuning of the relative contributions of transport and biosynthesis genes: a few molecules of biosynthetic enzymes could produce enough siderophore, but an excess in the level of the transport proteins benefits the cell in its chance encounter with ferric siderophore molecules in the extracellular environment (Salinas and Crosa 1995; Stork et al. 2007). We also showed that the promoter for RNAβ is active at both high and low iron concentrations and demonstrated by using *lacZ* transcriptional fusions to the *fatA–angR* intergenic region that the transcription termination event at the intergenic stem-loop, depends on the presence of RNAβ (Salinas and Crosa 1995; Stork et al. 2007). Using an in silico model of the RNAβ structure we further demonstrated the potential existence of at least four stem-loop structures and using site directed mutagenesis that loops I and II of RNAβ are directly involved and necessary for maximum termination to maintain the balance of transport

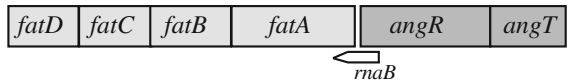

Fig. 1 Diagram of *fatD*, *C*, *B*, *A–angR*, *T* operon and location of antisense rnaB

versus biosynthesis gene transcripts (Stork et al. 2007). Mutations in either loop I or II changed the termination phenotype, and the complementary mutation restored the phenotype, indicating that these two loops might actually exist. Mutations in loop III or IV did not seem to eliminate or reduce termination, but they could simply not exist as part of RNAβ in the cell (Stork et al. 2007) (Fig. 1).

In this work we characterized the in vitro secondary structure of RNAβ and using a new in silico model we describe the effect of the loop mutations in the RNAβ structure.

Materials and methods

RNA preparations

RNAβ was synthesized using an in vitro transcription T7 kit (Ambion) and then purified by passage through a NucAway spin cleanup column (Ambion). The RNA was recovered using diethyl pyro carbonate (DEPC)-treated RNase-free water, and dephosphorylated before being end-labeled with 50 μ Ci (25 µl, 6,000 Ci/mmol ATP[γP^{32}] (Perkin Elmer). Both standard 5′ end labeling and 3′ end labeling using labeled pCp[P^{32}] were performed. Once labeled the RNA was run through a denaturing polyacrylamide gel electrophoresis (PAGE) and the labeled full-length product visualized by short exposure to film and eluted in gel elution buffer (Ambion) from a gel slice to exclude incomplete transcription and degraded products.

Hydrolysis ladder

This ladder was obtained by a partial hydrolysis of the sample resulting in a labeled band at every possible nucleotide. This allows for determination of the distance between each band and the conversion of gel information onto the sequence of the RNA. The prepared sample was placed in hydrolysis buffer to make a 1× solution of hydrolysis buffer and was then

heated to 95 °C in a heat block for 7 min. Several different time points were tried ranging from 2 to 15 and 7 min was found to produce the most even degradation products. The sample was removed from the heat block and hydrolysis was quenched with the addition of PAGE loading buffer and incubated on ice for several minutes. The sample was heated again in the heat block for 30 s immediately prior to loading in the gel.

T1 ladder

Prepared labeled sample was added to sequence buffer (Ambion) to make a 1× final solution of sequencing buffer, which reduces RNA folding. The sample was then heated at 50° for 5 min to denature the RNA structure and allow cleavage at all guanine bases. Without the denaturing step only exposed/unstructured Gs could be cleaved by the RNase as seen in the structure analysis with T1. 1 µl of Rnase T1 was added and incubated at room temperature for 15 min to produce a partial digestion of the labeled RNA that has been hydrolyzed at each G nucleotide. The digestion was quenched with addition of PAGE loading buffer and incubated on ice for several minutes. Reaction was heated to 95 °C for 30 s prior to loading to initially denature all structure. The partially digested RNA is then used as a control in order to tie the sequenced visualized on the gel to the known sequence of the sample RNA. All G nucleotides are visualized with this method, allowing localization of structure motifs seen on the gel to locations in the established sequence.

Structure analysis with T1 ribonuclease

The prepared labeled RNAβ sample was added to structure buffer (Ambion) to make a 1× final solution. The sample was then heated briefly to 50 °C and allowed to cool on ice for 2 min in order to promote correct and complete refolding of the RNA. No difference was detected when refolding took place at room temperature instead of on ice. At this point the sample was divided in half and either 0.1 or 0.01 µl Rnase T1 was added and allowed to partially digest for 5 min at room temperature (Tranguch et al. 1994). Digesting at 37 °C was found to promote extensive degradation and distinctive motifs were lost. Digestion was quenched with addition of PAGE loading buffer and placed on ice for several minutes. Digestion in the structure buffer leaves the RNA fully folded and only exposed and unstructured guanine bases are digested.

Structure analysis with V1 ribonuclease

V1 partial digests where prepared similar to T1 structure partial digests above, except that the concentration of enzyme was lower (0.01 and 0.001, respectively.) Partial digestion with V1 proved particularly sensitive to enzyme concentration compared to the other partial digestion methods. The digestion was allowed to proceed for 5 min before being quenched with PAGE loading buffer and incubated on ice for several minutes. The V1 enzyme digests only strongly base paired double stranded regions.

Structure analysis with lead acetate

Partial digestion with lead acetate was performed similarly to the T1 approach. Two samples of 9 µl each were prepared in structure buffer as above and allowed to refold. To these reactions 1 µl of lead acetate solution was added at either 25 or 50 mM concentration (Ciesiolka et al. 1993). Lead acetate cuts folded RNA molecules in unstructured loops and open regions. This reaction was allowed to proceed for 5 min before being quenched with the addition of PAGE loading buffer and incubation on ice (Fig. 2).

Polyacrylamide gel electrophoresis

PAGE was made using a 5 % concentration of acrylamide (19:1 acrylamide:bis). Gels were run for a variable period of time depending on the portion of the molecule to be visualized. Run times varied from 4 h for the 3′ and 5′ end portions to 20 h for the polymorphic region. Following PAGE, the gel was removed from the apparatus and dried briefly onto filter paper before being sealed in plastic wrap.

The gel was visualized by directly exposing the sealed gel to film for 15, 24 and/or 48 h at −80 °C in a sealed cassette, the length of time was varied depending on the intensity of the resulting bands. Generally more than one exposure time was used. The film used was Kodak 35 × 45 cm high sensitivity film and developed in an automatic developer. The location of structural features present in the partial digestion lanes was determined using the T1 sequence ladder bands and the hydrolysis ladder. When compared against

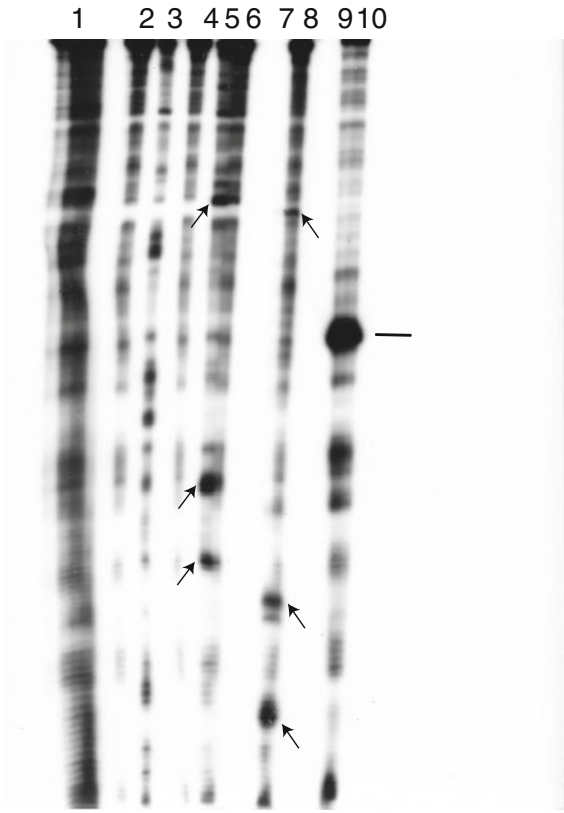

Fig. 2 Structure sequence after RNase and lead acetate treatment of RNAβ. Lanes *left to right* are *1* hydrolysis ladder, *2* T1 ladder, *3* undigested control, *4* 1 µl T1 structure digest, *5* 0.1 µl T1 digest, *6* 0.01 µl T1 digest, *7* 0.1 µl V1 digest, *8* 0.01 µl V1 digest, *9* 1 µl of 50 mM lead acetate, *10* 1 µl of 25 mM lead acetate. *Arrows* indicate points of digestion in RNase T1 and V1 lanes. *Line* indicates the unusual strong point of digestion in lead acetate lanes. Samples were run for 15 h to obtain this pattern

known sequence these lanes allow for placement of other bands onto the known sequence in the correct location and for the determination of structural motifs.

lacZ fusions

The *lacZ* fusion construct pMDL125 was made using the native cut sites *Hin*dIII–*Pst*I, the cloned portion includes the 3′ end of *fatA*, the intergenic region and the 5′ end of *angR* was cloned into broad range vector pKT231, from which a *Bst*EII–*Sal*I fragment was moved into pTL61T upstream of the *lacZ* gene to create the fusion (Bagdasarian et al. 1981). This plasmid was then subjected to site directed mutagenesis at the *rnaB*-10 promoter region to reduce expression of RNAβ resulting in plasmid pMS125. Constitutive RNAβ expression was achieved by creating a 430 nucleotides *rnaB* fragment without its natural promoter originated from a *Sna*BI–*Afl*III fragment of pJM1 that was ligated into pACYC184 resulting in pSC45. Loop mutations were obtained by site directed mutagenesis in pSC45 to determine the effects of mutation on pMS125 *lacZ* expression. Mutations were carried out using the Quickchange site directed mutagenesis kit (stratagene) according to the manufacturer's recommendations. All mutants were sequenced prior to conjugation to verify that the only bases affected were ones induced by site directed mutagenesis. Construction of pSC45-L1C/L2C was made by back-to-back mutagenesis of pSC45, first for loop I, then loop II.

Results

A purified PCR product of the RNAβ region was produced using specific primers to include a T7 promoter upstream of the antisense RNA indigenous promoter. This PCR product was then transcribed and the resulting RNA end-labeled with P^{32} at both the 5′ and 3′ ends. These approaches had to be used to determine the structure from opposite ends of the RNA molecule because the 427 base pair RNAβ is too long to allow for structure determination solely from one end of the molecule. The labeled RNA was then partially digested with RNases specific for single or double stranded RNA (Tranguch et al. 1994) or lead acetate that is specific for single stranded RNA regions used in hydrolysis buffer (Ciesiolka et al. 1993). As described in the Methods section, these reactions were allowed to continue for a determined amount of time before being quenched with loading buffer and incubated on ice before loading and run on a denaturing PAGE as shown in Fig. 2.

The generated in vitro structure data indicated that three of the four previously described four loops were in agreement with the original model, however the alteration of loop IV as well as several other structural differences in the overall shape of the molecule led to the necessity of creating a new model. The new model (Fig. 3) was created using the online program Mfold version 2.3, which despite being a slightly dated folding program allows for predictions at a specified temperature of 25 °C, the normal growth temperature

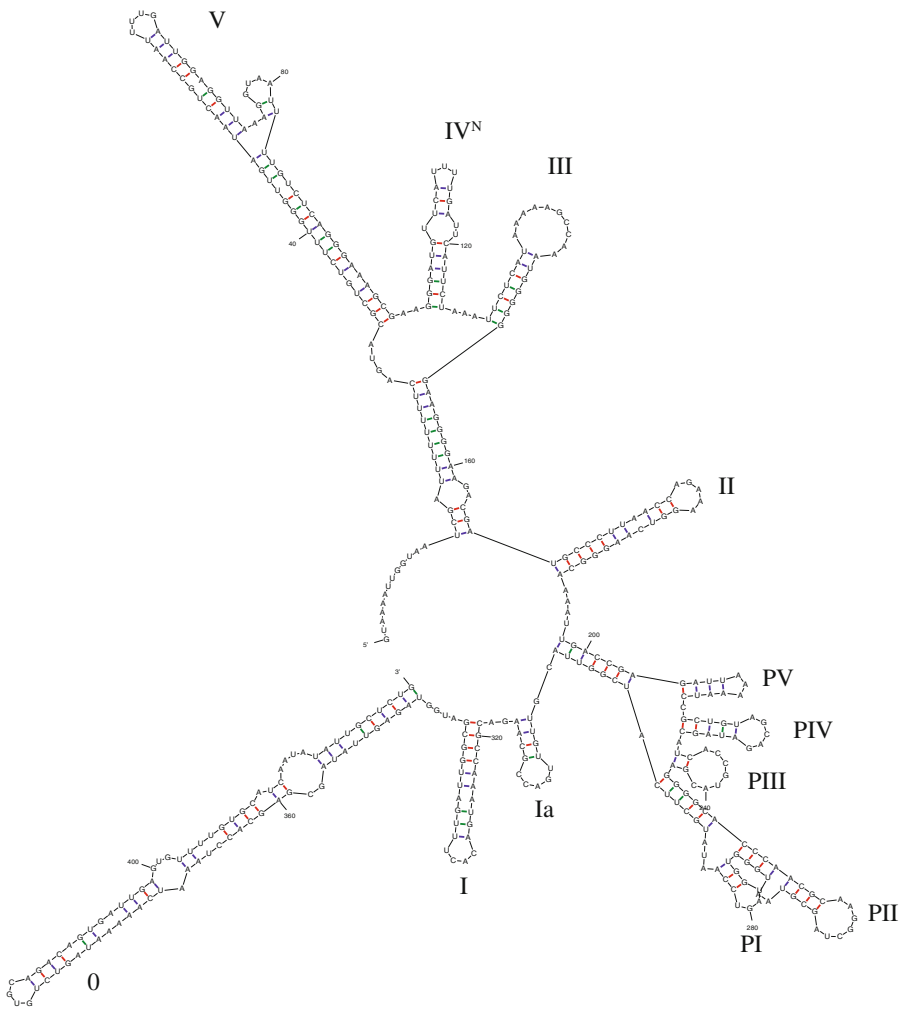

Fig. 3 In silico predicted structure of RNAβ using Mfold version 2.3 at 25 °C and default energies

of *Vibrio anguillarum.* This model was different in backbone construction from the previously published model, however many important features are conserved between them such as three of the four loops previously identified in the previous work (source). The stem-loops of the new model were given new names with the names given in the previously named model maintained for continuity. Loop IV as described in previous work is heavily modified from that form in this model and is worthy of immediate note. To avoid confusion this loop has been named loop IV^N in the current structure to indicate the change.

The loops in the new model were named from the 3′ end towards the 5′ end in keeping with the original work. Loops between the small Ia and loop II are in a region from which little structural information could be obtained and seems to be polymorphic in nature. The majority of models produced have tremendous variability in this region (data not shown), thus the label of 'P' with all the stem-loops in this region describe some uncertainties on the structure of this region.

The initial sequencing experiments from the 5′ end indicate that the overall structure of the model must be correct with the large leading stem-loop V, however several differences in the T1 and lead acetate digests were observed. All data points from all digests were carefully mapped to the model and the in silico prediction was adjusted slightly as five discrepancies were found. Four out of five of these discrepancies were easily corrected for and involved creating small, unstructured regions or extending existing loops (Fig. 5). The fifth discrepancy between the model and the experimental data was at the end of loop I

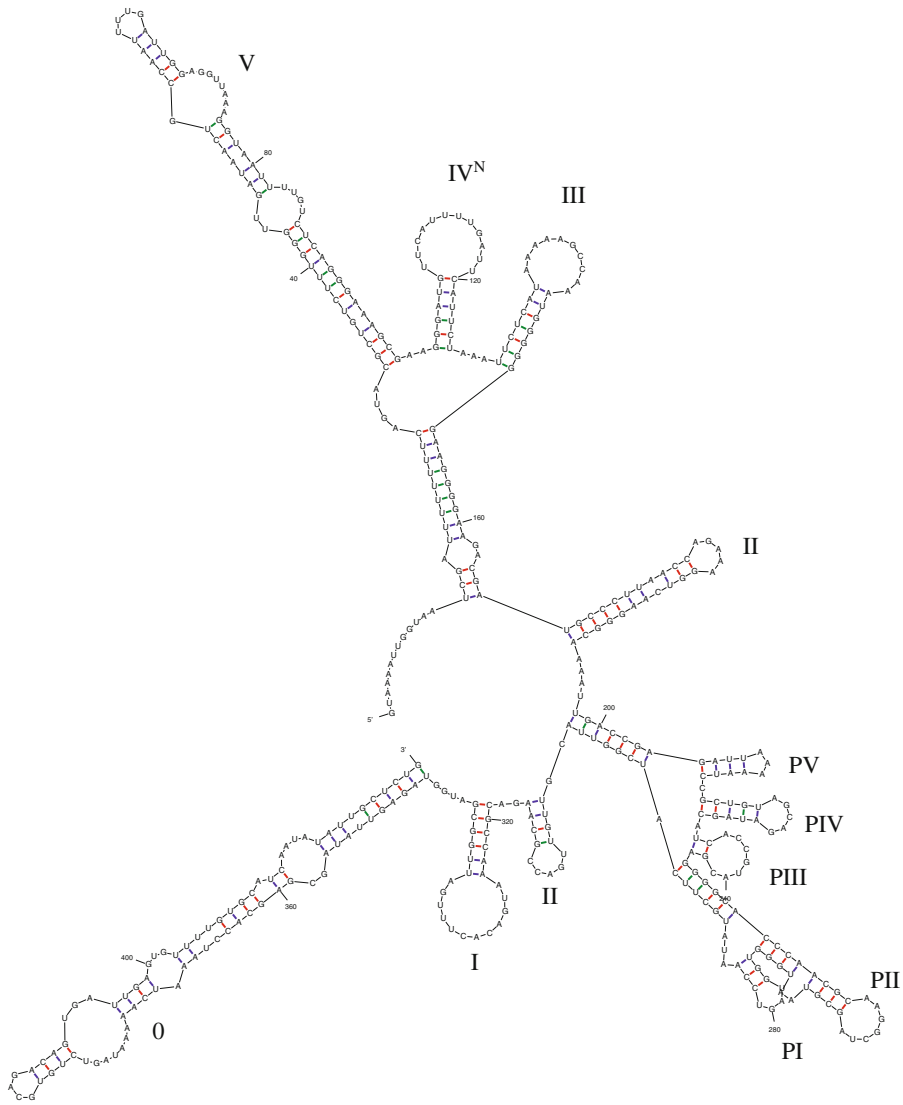

Fig. 4 In vitro solved structure. This differs from the model in Fig. 1 in loops 0, I, IV^N and V with all four regions changing from paired to unpaired regions

where the V1 digest indicated that the exposed end of loop I was strongly bound and double stranded. We were unable to model this in a manner consistent with the other data points, however this substructure could be obtained if the polymorphic region folds over and the end of loop PI pairs with the end of loop I that cannot be seen in this model based only on secondary structure analysis.

There is a possibility for alternative interpretation of the data in loop IV^N that would lead to a slightly different structure. Lead acetate digestion (Ciesiolka et al. 1993) at base pairs 115–117 in loop IV^N results in a more intense band and is a preferred cleavage site over other lead acetate cleavage locations in the molecule. This preferred cleavage may indicate that instead of being unstructured and single stranded as shown in Fig. 4. The location is instead a magnesium binding site, as it has been established that Mg^{2+} binding sites also bind Pb^{2+} from lead acetate and triggers cleavage at the binding location (Streicher et al. 1993; Pan 2001). If this is the case the structure is likely that of the in silico prediction found in Fig. 3 instead of the open loop shown in Fig. 4. The single G base present in the open loop is insufficient to conclude by T1 digestion if the base is exposed since a faint band was present at this location in all lanes, indicating a natural site of degradation but making further analysis impossible with this method.

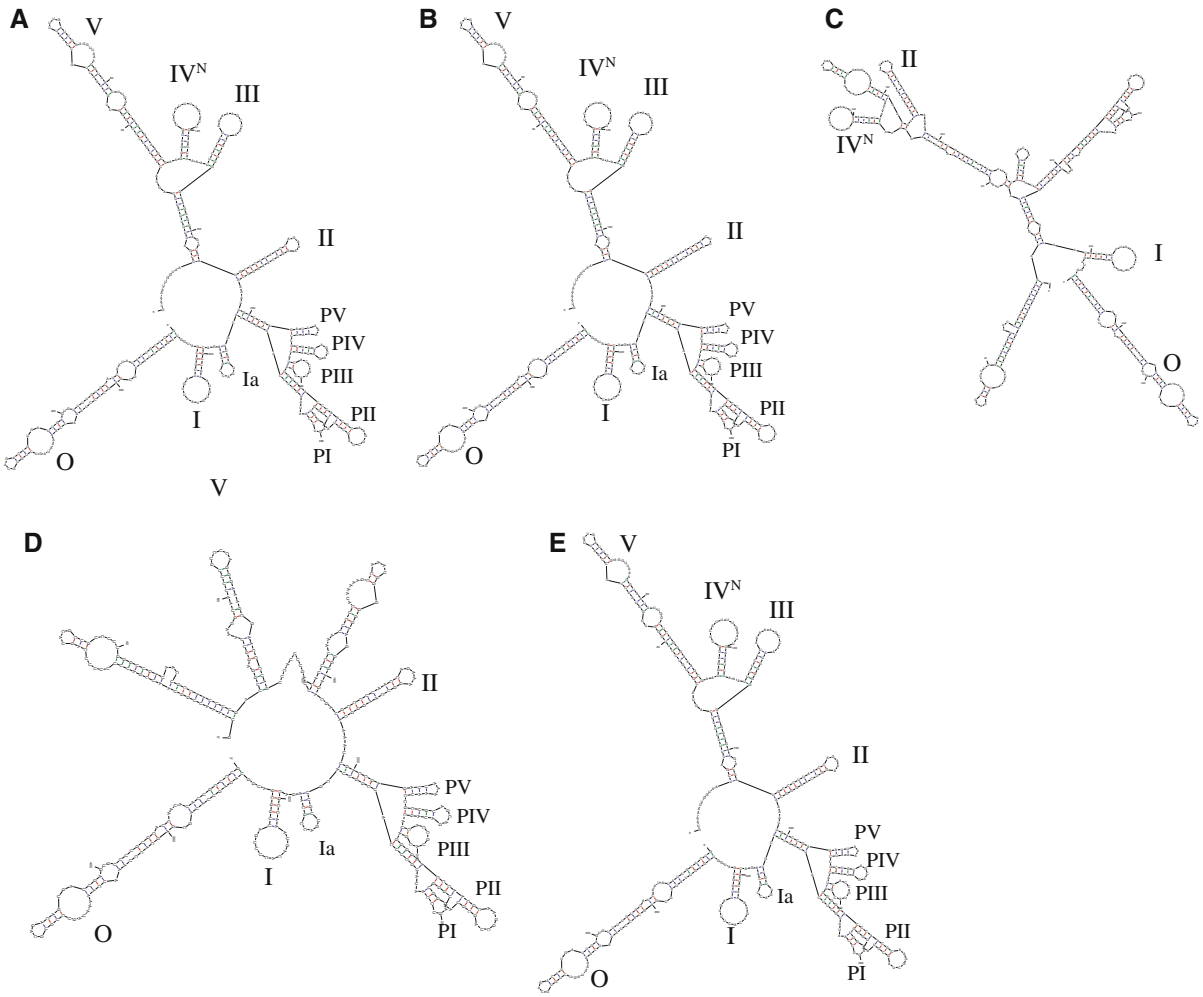

Fig. 5 In silico predicted structures of the effects of side directed mutations in the end of possible function loops to complement sequences using the model corrected for the observed data. **a** Loop I mutation, no predicted structural change. **b** Loop II complementary expression mutation. Minimal predicted change. **c** Loop III mutation. Significant predicted changes of structural backbone, loops I, II, and IV^N remain intact. **d** Loop IV mutation. First 167 base pairs of structure predicted to change, including loss of loops V, IV^N, and III. Remainder of structure is predicted to be identical to the wild type. **e** Wild type structure included for comparison

The previously generated mutations in a selection of these loops based on the original model were previously analyzed (Stork et al. 2007) using β-galactosidase assays. Table 1 shows a summary of the previous β-galactosidase results (Stork et al. 2007). Plasmid pMDL125 was constructed by fusing the 3′ end of *fatA*, the intergenic region, and the 5′ end of *angR* made using a *Hin*dIII–*Pst*I fragment to the promoterless *lacZ* gene from plasmid pTL61T (Linn and Pierre 1990). This plasmid served as a recreation of wild type expression as both RNAβ and the target mRNA sequence are present. When RNAβ was expressed antisense, β-galactosidase expression dropped (Table 1, row 1). Since we were unable to generate a RNAβ knockout, pMDL125 was used to generate a site directed mutation in the −10 promoter of *rnaB* to reduce transcription resulting in plasmid pMS125. This mutation has significantly increased β-galactosidase expression, which was reduced to wild type levels by the addition in trans of constitutively expressed RNAβ from plasmid pSC45 containing the *rnaB* gene in trans (Table 1, rows 2, 3). The pSC45 plasmid was subjected to further directed mutagenesis to create mutations in loop I, II, III or IV.

Table 1 Summary of previous *fatA–angR* β-galactosidase fusions under effects of differing RNAβ sources

Row	Plasmid	pSC45	Miller units	Standard deviation
1	pMDL125	–	1,486	114.3
2	pMS125	–	4,971	285.7
3	pMS125	+	1,086	171.4
4	pMS125	L1C	2,400	114.3
5	pMS125	L2C	2,286	128.6
6	pMS125	L3C	343	28.6
7	pMS125	L4C	400	42.9
8	L1C	–	4,571	314.3
9	L2C	–	4,343	514.3
10	L1C	+	2,286	114.3
11	L2C	+	2,514	142.9
12	L1C	L1C	1,257	100
13	L2C	L2C	1,229	102.86
14	L1C/L2C	L1C/L2C	4,543	400

There are no in silico predicted structural changes resulting from the mutation of loop I. The mutation (ACACU to TGTAA) causes a noticeable decrease in β galactosidase expression in vivo (Table 1) indicating that loop I is likely involved in interaction with the mRNA substrate. Data obtained from V1 partial digests indicate that this region is actually double stranded and does not match the model, however no models could be created that contained both this region as double stranded and the other structural features seen with the rest of the data. Mutation of loop II to the complementary bases (GAAA to CTTT) has only a small effect on the predicted structure, since the only predicted structural change is the tightening and reduction of the end of loop II. Wild type RNAβ has five unstructured bases (AGAAA) while the complement mutation has only 3 (CUU) the last U introduced by the mutation of the base pairs with the unchanged A left in the free loop and resulting in tightening of the stem. No other structural changes are predicted to take place with these mutations according to in vitro modeling. Previously performed in vitro β-galactosidase experiments show a decrease in RNAβ function when loop II is mutated to the complement sequence (Table 1, row 5) rationalizing the importance of loop II for interaction with the mRNA target (Stork et al. 2007). Mutation of loop III to the complementary bases (AAGCC to TTCGG) causes significant structural rearrangement in the model. Loop III changes result in the end of the loop becoming double stranded and a small new loop is generated (Fig. 5). Loop IV^N, II and I are both preserved in structure, but the location of loop II is moved in relation to loop I and the polymorphic region between them becomes more orderly. Several structural features are missing in this mutation that are present in both the model and the in vitro data. The originally described loop IV does not exist in the new model. This is instead the region making one side of the stem of a small stem-loop structure very similar in size to loop III. Mutation of this sequence (GGGAU to CCCUA), all of which is fully base paired to form the stem of this local structure, is predicted to disrupt the first 167 base pairs of the structure including loop III, however the remainder of the structure is identical to the wild type. The mutations in both loop III and IV lead to an increased activity of RNAβ in vivo (Table 1, row 6, 7) as compared to wild type.

Discussion

Prediction of the RNA molecules with a different configuration are also shown in Fig. 5. RNAs are emerging as regulators that enable bacterial pathogens to express genes when required during their life cycle. Numerous small RNAs are implicated in the regulation of infections caused by Gram-positive and negative bacteria (Gottesman 2004). These post-transcriptional regulators can regulate the expression of genes encoded by plasmid and chromosomes with some of them regulating the expression of virulence genes. Antisense RNAβ, a plasmid-encoded regulatory antisense RNA expressed by *V. anguillarum* being 427 nucleotide-long is not a particularly small RNA although it compares well to the 519 nucleotide-long RNA III, the first RNA shown to be involved in bacterial pathogenesis (Salinas et al. 1993, 1995; Hershberg et al. 2003; Balaban and Novick 1995). These two RNAs are 4–5 times bigger than most small RNAs. The action of RNAβ on the ITB operon mRNA proceeds by antisense pairing subsequently blocking transcription elongation. The consequence is that RNAβ affects the transcription process at a stem-loop structure located in the intergenic region between the *fatA* and *angR* genes of the ITB operon, thus this gene regulation is likely to be irreversible. The net result is a higher level of the *fatD*, *fatC*, *fatB*, and *fatA* moiety as

compared with the longer transcript encoding those genes as well as the *angR* and *angT* genes.

In this work, we report the synthesis of RNAβ and its labeling at both the 5′ and 3′ ends. It was necessary to label the RNA at both ends because of its large size. We determined structural features by treatment of RNAβ with single and double strand specific ribonucleases as well as lead acetate followed by sequencing. The generated in vitro structural data indicated that three of the four previously described loops were in agreement with the original model (Stork et al. 2007), however the alteration of loop IV as well as several other structural differences in the overall shape of the molecule led to the necessity of creating a new in silico model. Using the sites of mutations in the various loops we modeled the change in the RNAβ secondary structure induced by those mutations. Mutations of loops III and IV to their complementary bases alter the overall structure of the RNA significantly but increase its function of transcriptional termination while mutations to loops I and II have the opposite effect, the structure is unchanged but the activity decreases as shown by an increase in β-galactosidase activity (Stork et al. 2007). This suggests that loops I and II are necessary for interaction with the target mRNA leading to a transcription termination event (Stork et al. 2007; Yarnell and Roberts 1999). This hypothesis was confirmed by corresponding complementary mutations in the corresponding β-galactosidase mRNA fusion target sequences that restored RNAβ activity to wild type levels. It is possible that the structural rearrangement introduced by mutations in loops III and IV promotes activity and binding of loops I and II through reducing steric hindrance or increased binding to the target. This result also indicates that the exact relative positions of the critical loops are unimportant for activity. The potential binding between the polymorphic loop PI and I is unimportant as well as it is abolished in loops III and IV mutations. One feature is present in the data that is not indicated in this model. The end portion of stem-loop I have three nucleotides (AC**ACU**UU) that are indicated by the V1 partial digest to be strongly base paired. We were unable to generate a model of this feature that was in compliance with the numerous other data points and this indicates a possibility that the bonding is formed within the tertiary structure since this region is complementary to the end of loop PI in the polymorphic region.

The secondary structure described in this work has helped to pinpoint functional domains of this antisense RNA that interact with the ITB operon mRNA. It remains to be determined whether RNAβ function is pleiotropic affecting the expression of other chromosomal and/or plasmid genes in addition to those in the ITB operon since due to its larger size this RNA could be interacting with multiple partners.

References

Actis LA, Tolmasky ME, Farrell DH, Crosa JH (1988) Genetic and molecular characterization of essential components of the *Vibrio anguillarum* plasmid-mediated iron-transport system. J Biol Chem 263:2853–2860

Bagdasarian M, Lurz R, Ruckert B, Franklin FC, Bagdasarian MM, Frey J, Timmis KN (1981) Specific-purpose plasmid cloning vectors II. Broad host range, high copy number, RSF1010-derived vectors, and a host-vector system for gene cloning in *Pseudomonas*. Gene 16:237–247

Balaban N, Novick RP (1995) Translation of RNAIII, the *Staphylococcus aureus* agr regulatory RNA molecule, can be activated by a 3′-end deletion. FEMS Microbiol Lett 133:155–161

Chai S, Welch TJ, Crosa JH (1998) Characterization of the interaction between fur and the iron transport promoter of the virulence plasmid in *Vibrio anguillarum*. J Biol Chem 273:33841–33847

Chen Q, Crosa JH (1996) Antisense RNA, fur, iron, and the regulation of iron transport genes in *Vibrio anguillarum*. J Biol Chem 271:18885–18891

Chen Q, Wertheimer AM, Tolmasky ME, Crosa JH (1996) The *angR* protein and the siderophore anguibactin positively regulate the expression of iron-transport genes in *Vibrio anguillarum*. Mol Microbiol 22(1):127–134

Ciesiolka J, Michalowski D, Wrzesinski J, Krajewski J, Krzyzosiak WJ (1993) Patterns of cleavages induced by lead ions in defined RNA secondary structure motifs. J Mol Biol 275:211–220

Gottesman S (2004) The small RNA regulators of *Escherichia coli*: roles and mechanisms. Annu Rev Microbiol 58: 303–328

Hershberg R, Altuvia S, Margalit H (2003) A survey of small RNA-encoding genes in *Escherichia coli*. Nucleic Acids Res 31:1813–1820

Linn T, St. Pierre R (1990) Improved vector system for constructing transcriptional fusions that ensures independent translation of *lacZ*. J Bacteriol 172:1077–1084

Pan T (2001) Probing RNA structure by lead cleavage. Curr Protoc Nucleic Acid Chem 6(6):3

Salinas PC, Crosa JH (1995) Regulation of *angR*, a gene with regulatory and biosynthetic functions in the pJM1 plasmid-mediated iron uptake system of *Vibrio anguillarum*. Gene 160:17–23

Salinas PC, Tolmasky ME, Crosa JH (1989) Regulation of the iron uptake system in *Vibrio anguillarum*: evidence for a

cooperative effect between two transcriptional activators. Proc Natl Acad Sci USA 86(10):3529–3533

Salinas PC, Waldbeser LS, Crosa JH (1993) Regulation of the expression of bacterial iron transport genes: possible role of an antisense RNA as a repressor. Gene 123:33–38

Stork M, Di Lorenzo M, Welch TJ, Crosa JH (2007) Transcription termination within the iron transport-biosynthesis operon of *Vibrio anguillarum* requires an antisense RNA. J Bacteriol 189:3479–3488

Streicher B, Ahsen UV, Schroeder R (1993) Lead cleavage sites in the core structure of group I intron-RNA. Nucleic Acids Res 21:317–331

Tolmasky ME, Wertheimer AM, Actis LA, Crosa JH (1994) Characterization of the *Vibrio anguillarum* fur gene: role in regulation of expression of the *fatA* outer membrane protein and catechols. J Bacteriol 176(1):213–220

Tranguch AJ, Kindelberger DW, Rohlman CE, Lee JY, Engelke DR (1994) Structure-sensitive RNA footprinting of yeast nuclear ribonuclease P. Biochemistry 33:1778–1787

Wertheimer AM, Verweij W, Chen Q, Crosa LM, Nagasawa M, Tolmasky ME, Actis LA, Crosa JH (1999) Characterization of the *angR* gene of *Vibrio anguillarum*: essential role in virulence. Infect Immun 67:6496–6509

Yarnell WS, Roberts JW (1999) Mechanism of intrinsic transcription termination and antitermination. Science 284: 611–615